SCIENCE CHINA
Information Sciences

• RESEARCH PAPER •

August 2025, Vol. 68, Iss. 8, 180502:1–180502:11
https://doi.org/10.1007/s11432-025-4500-8

Special Topic: Quantum Information

Direct estimation of quantum channel incompatibility via a quantum switch

Yuyan WEI[1,2], Gong-Chu LI[1,2], Li-Wen WANG[1,2], Xu-Song HONG[1,2], Lei CHEN[1,2], Si-Qi ZHANG[1,2], Hua-Qin XU[1,2], Yuancheng LIU[1,2], Yong-Sheng ZHANG[1,2,3,4*], Geng CHEN[1,2,3,4*], Chuan-Feng LI[1,2,3,4*] & Guang-Can GUO[1,2,3,4]

[1] *CAS Key Laboratory of Quantum Information, University of Science and Technology of China, Hefei 230026, China*
[2] *Anhui Province Key Laboratory of Quantum Network, Hefei 230026, China*
[3] *CAS Center For Excellence in Quantum Information and Quantum Physics, University of Science and Technology of China, Hefei 230026, China*
[4] *Hefei National Laboratory, Hefei 230088, China*

Received 11 April 2025/Revised 3 June 2025/Accepted 16 June 2025/Published online 8 July 2025

Abstract Incompatibility is a fundamental feature of the quantum world, with the incompatibility of observables famously captured by the Heisenberg uncertainty principle. As a matter of fact, the quantum channel incompatibility (QCI) renders a more valuable insight and wider scope into the incompatibility, in the light that the incompatibility essentially originates from the disturbance of the eigenstates imposed by a quantum channel. However, characterizing QCI remains challenging since it is intractable to apply two channels in alternative orders simultaneously on the same quantum system. A recent theoretical proposal [Phys. Rev. Lett. 130, 170201 (2023)] introduced a general definition of QCI based on measurement processes and showed that a quantum switch (QS), an implementation of indefinite causal order (ICO), can enable direct estimation of QCI. The quantum switch, already known for its applications in quantum communication, metrology, and quantum thermodynamics, offers a powerful tool for probing such process-level incompatibilities. In this work, we experimentally measure the incompatibility of several quantum noise channels, including depolarizing, bit-flip, and phase-flip channels, using a Sagnac-type quantum switch. Furthermore, we demonstrate that estimating QCI via ICO provides substantial improvements in resource efficiency over traditional process tomography approaches. Our results demonstrate that the quantum switch not only offers quantum advantages in information processing but also serves as a versatile platform for investigating fundamental aspects of quantum mechanics.

Keywords quantum channel incompatibility, quantum switch, quantum information, indefinite causal order

Citation Wei Y Y, Li G-C, Wang L-W, et al. Direct estimation of quantum channel incompatibility via a quantum switch. Sci China Inf Sci, 2025, 68(8): 180502, https://doi.org/10.1007/s11432-025-4500-8

1 Introduction

Observables form the foundation of physics, and in quantum mechanics, the concept of incompatible observables plays a fundamental role. The inability to precisely measure certain observables simultaneously is a defining feature that sets quantum mechanics apart from classical physics. This so-called incompatibility underpins essential quantum phenomena, including complementarity [1], quantum nonlocality [2–4], and contextuality [5–7]. Beyond its foundational significance, incompatibility is also a crucial resource in quantum information science, influencing applications such as quantum cryptography and quantum metrology. At the heart of observable incompatibility lies the non-commutativity of quantum operators ($\hat{A}$ and $\hat{B}$), expressed as $[\hat{A}, \hat{B}] \neq 0$. This algebraic structure enforces the Heisenberg uncertainty principle [8], which places a lower bound on the measurement precision of two noncommuting observables that $\sigma(A)\sigma(B) \geqslant \frac{\hbar}{2}\langle[\hat{A}, \hat{B}]\rangle$, where σ represents the standard deviation. This principle quantifies the fundamental limitation in simultaneously measuring two observables. Later, in an effort to account for measurement-induced disturbance, rigorous and general theoretical treatments of quantum measurements revealed the limitations of Heisenberg's original relation. As a result, a new, universally valid uncertainty relation was derived [9–12], which refines the uncertainty principle by incorporating both the

* Corresponding author (email: yshzhang@ustc.edu.cn, chengeng@ustc.edu.cn, cfli@ustc.edu.cn)

© Science China Press 2025

measurement error and the corresponding disturbance. While the incompatibility of observables primarily concerns changes in expectation values, specifically, the changes in the projection probabilities. These changes ultimately originate from deeper structural transformations—the disturbance of the system's eigenstates after passing a quantum channel. In this sense, quantum channel incompatibility (QCI) represents a more fundamental layer of quantum incompatibility, serving as the underlying source from which observable incompatibility emerges. Various theoretical measures for the incompatibility of channels have been proposed, including robustness to noise [13–16] and the influence of incompatible channels in specific quantum tasks or processes [17–19]. Although previous studies have significantly advanced the study of incompatibility, they still face two main limitations. First, they often involve complex optimization procedures [13–21], which are difficult to implement in practical experimental settings. Second, due to the fundamental impossibility of applying two quantum channels simultaneously to the same system and directly observing their mutual disturbance, there exists no straightforward method to directly quantify the incompatibility of quantum channels [22–27]. A promising solution to this problem emerges from the framework of indefinite causal order (ICO). This structure enables a form of superposition of causal orders, offering advantages in computational complexity and information processing [28–33]. Based on this idea, Gao et al. [34] proposed a method to estimate QCI by leveraging the quantum switch. Their approach allows for the simultaneous evaluation of how one channel $\mathcal{A}$ affects an observable $\hat{B}$ and how another channel $\mathcal{B}$ affects an observable $\hat{A}$. This method extends beyond unitary channels and can be applied to general quantum processes, including the quantum noise channels. In this study, we first give an introduction to the incompatibility of quantum channels and then present an experimental demonstration of direct QCI estimation using the quantum switch. We apply this method to fundamental quantum noise channels, such as depolarization, bit-flip, and phase-flip channels, providing a practical approach to assessing incompatibility without relying on indirect statistical reconstructions. Furthermore, we demonstrate that, compared to process tomography, our ICO-based method provides a more efficient and direct means of probing QCI. Our implementation is based on a Sagnac-type quantum switch, which ensures high coherence and spatial mode stability, allowing for precise measurements.

2 Review of indefinite causal order

In quantum information science, the standard circuit model is characterized by the assumption that quantum gates are applied in a fixed sequence. In contrast, the concept of ICO introduces a different paradigm in which the order of quantum operations is not predetermined. This novel approach enables quantum systems to exhibit advantages over classical and even conventional quantum circuits. Specifically, it facilitates an exponential reduction in communication complexity [35], achieves a super-Heisenberg limit in metrology [36], and enhances refrigeration cycles [37].

The notion of indefinite causal order was first introduced through the quantum switch [28, 29], as defined by

$$\begin{aligned}\mathrm{QS}(|\psi\rangle\otimes|+\rangle) =&\frac{1}{\sqrt{2}}\big(\mathcal{BA}|\psi\rangle|0\rangle+\mathcal{AB}|\psi\rangle|1\rangle\big)\\ =&\mathrm{e}^{\mathrm{i}\phi}\mathcal{AB}|\psi\rangle\otimes\frac{1}{\sqrt{2}}(\mathrm{e}^{\mathrm{i}\phi}|0\rangle+\mathrm{e}^{-\mathrm{i}\phi}|1\rangle)\\ =&\mathrm{e}^{\mathrm{i}\phi}\mathcal{AB}|\psi\rangle\otimes(\cos\phi|+\rangle+\mathrm{i}\sin\phi|-\rangle),\end{aligned}\tag{1}$$

where $\mathcal{A}$ and $\mathcal{B}$ are unitary operations satisfying $\mathcal{AB}=\mathrm{e}^{-2\mathrm{i}\phi}\mathcal{BA}$. Here, $\mathrm{QS}(\cdot)$ represents the quantum switch, $|\psi\rangle$ is the input state, and the control qubit is prepared in the superposition state $|+\rangle=\frac{1}{\sqrt{2}}(|0\rangle+|1\rangle)$. Measuring the control qubit in the basis of $\{|+\rangle,|-\rangle\}$ allows one to determine whether the unitaries commute ($\phi=0$) or anti-commute ($\phi=\pi/2$). The quantum switch can be generalized to non-unitary quantum channels [38]. Suppose the input state ρ has dimension d, and the quantum channels $\mathcal{A},\mathcal{B}:\mathcal{H}_d\to\mathcal{H}_d$ are described by their Kraus representations $\mathcal{A}(\cdot)=\sum_i A_i(\cdot)A_i^\dagger$ and $\mathcal{B}(\cdot)=\sum_j B_j(\cdot)B_j^\dagger$ with constraints of $\sum_i A_i^\dagger A_i=I$ and $\sum_j B_j^\dagger B_j=I$. For a control qubit initialized as $\omega=|+\rangle\langle+|$, the output state after the quantum switch is given by

$$\mathrm{QS}(\rho\otimes\omega)=\big(\mathcal{B}\circ\mathcal{A}\otimes|0\rangle\langle0|+\mathcal{A}\circ\mathcal{B}\otimes|1\rangle\langle1|\big)(\rho\otimes\omega).\tag{2}$$

Here, $\mathcal{A} \circ \mathcal{B}(\cdot) = \mathcal{A}(\mathcal{B}(\cdot))$. Using the Kraus decomposition, this expression can be rewritten as

$$\begin{aligned}\mathrm{QS}(\rho \otimes \omega) = \frac{1}{4}\sum_{ij} \big(&\{A_i, B_j\}\rho\{A_i, B_j\}^\dagger \otimes \omega + \{A_i, B_j\}\rho[A_i, B_j]^\dagger \otimes \omega Z \\ &+ [A_i, B_j]\rho\{A_i, B_j\}^\dagger \otimes Z\omega + [A_i, B_j]\rho[A_i, B_j]^\dagger \otimes Z\omega Z\big).\end{aligned} \tag{3}$$

Here $Z = |0\rangle\langle 0| - |1\rangle\langle 1|$ is the Pauli Z operator, and $[A, B] = AB - BA$, $\{A, B\} = AB + BA$. Notably, when all Kraus operators of $\mathcal{A}$ and $\mathcal{B}$ commute, the $Z\omega Z$ term vanishes, indicating perfect compatibility between the channels.

3 Incompatibility of quantum channels

Suppose we have two observables, $\hat{A}$ and $\hat{B}$, each composed of eigenvalues and eigenspaces: $\hat{A} = \sum_i a_i A_i, \hat{B} = \sum_j b_j B_j$. Here, a_i and b_j are eigenvalues, while A_i and B_j represent the corresponding projection spaces. If the projection spaces satisfy $\mathrm{rank}(A_i) = 1$, then $A_i = |a_i\rangle\langle a_i|$, and the measurement is a projective measurement. The same applies to $\hat{B}$. Each observable corresponds to a measurement process. For projective measurements of $\hat{A}$ and $\hat{B}$, the measurement processes on an input state ρ are given by $\mathcal{A}(\rho) = \sum_i \langle a_i|\rho|a_i\rangle |a_i\rangle\langle a_i|$ and $\mathcal{B}(\rho) = \sum_j \langle b_j|\rho|b_j\rangle |b_j\rangle\langle b_j|$.

More generally, for the cases with $\mathrm{rank}(A_i) \geqslant 1$ and $\mathrm{rank}(B_j) \geqslant 1$, the measurement processes for $\hat{A}$ and $\hat{B}$ can be expressed as

$$\begin{cases}\mathcal{A}(\rho) = \sum_i A_i \rho A_i^\dagger, \\ \mathcal{B}(\rho) = \sum_j B_j \rho B_j^\dagger.\end{cases} \tag{4}$$

These measurement processes satisfy the Kraus representation of a general quantum channel. Hereafter, we will not distinguish the measurement process $\mathcal{A}$ and the general quantum channel $\mathcal{A}$.

If the two processes commute with each other, each pair of Kraus operators must also commute, i.e., $[\mathcal{A}, \mathcal{B}] = 0 \Rightarrow [A_i, B_j] = 0,\ \forall i, j$. Any two of the Kraus operators that are not commuting indicate the incompatibility between these two quantum channels. To quantify the incompatibility, we focus on how much the state remains within the original subspace, as characterized by the overlap between the states before and after the channel.

Now, consider that the system is initially in an eigenstate of $\hat{A}$, defined as $|\alpha_i\rangle$, selected uniformly at random from the ith eigenspace. The index i follows the probability distribution $p_i := d_{A,i}/d$, where $d_{A,i}$ is the dimension of the eigenspace and d is the dimension of the entire space. The system then undergoes a measurement process associated with $\hat{B}$. Given an outcome j, the probability is $p_b(j) = \langle \alpha_i|B_j|\alpha_i\rangle$, and the system collapses into the state $B_j|\alpha_i\rangle / \|B_j|\alpha_i\rangle\|$. Averaging over all outcomes, the post-measurement system state becomes

$$\sum_j p_b(j) \frac{B_j|\alpha_i\rangle\langle\alpha_i|B_j}{\|B_j|\alpha_i\rangle\|^2}. \tag{5}$$

With the definition of the quantum channel $\mathcal{B}(\rho) := \sum_j B_j \rho B_j$, the corresponding state can be rewritten as $\mathcal{B}(|\alpha_i\rangle\langle\alpha_i|)$. Finally, performing a measurement of $\hat{A}$, the probability of obtaining outcome i is given by $\mathrm{Tr}[A_i \mathcal{B}(|\alpha_i\rangle\langle\alpha_i|)]$. Averaging over all possible initial states, the probability that the system remains in the original eigenspace is

$$\begin{aligned}\mathrm{Prob}(\hat{A}, \mathcal{B}) :=& \sum_i p_i \int \pi_i(d\alpha_i)\, \mathrm{Tr}[A_i \mathcal{B}(|\alpha_i\rangle\langle\alpha_i|)] \\ =& \frac{1}{d}\sum_{ij} \mathrm{Tr}[A_i B_j A_i B_j].\end{aligned} \tag{6}$$

Here, $\pi_i(d\alpha_i)$ represents the uniform probability distribution over pure states in the ith subspace. The initial system state is given by $\rho = \sum_i p_i \int \pi_i(d\alpha_i)|\alpha_i\rangle\langle\alpha_i|$.

It can be proven that this probability is symmetric,

$$\mathrm{Prob}(\hat{A}, \mathcal{B}) = \mathrm{Prob}(\mathcal{A}, \hat{B}). \tag{7}$$

Based on this, Ref. [34] introduces a measure of QCI defined as $\mathrm{QCI}(\mathcal{A},\mathcal{B}) := \sqrt{1-\mathrm{Prob}(\hat{A},\mathcal{B})} = \sqrt{1-\mathrm{Prob}(\hat{B},\mathcal{A})}$, i.e.,

$$\mathrm{QCI}(\mathcal{A},\mathcal{B}) = \sqrt{1-\frac{1}{d}\sum_{ij}\mathrm{Tr}[A_iB_jA_iB_j]}. \tag{8}$$

This definition extends naturally from the measurement processes for observables $\hat{A}$ and $\hat{B}$ to general quantum channels $\mathcal{A}$ and $\mathcal{B}$ through their Kraus representations.

Such measure satisfies several key properties [34]: (1) symmetry, i.e., $\mathrm{QCI}(\mathcal{A},\mathcal{B}) = \mathrm{QCI}(\mathcal{B},\mathcal{A})$; (2) non-negativity, i.e., $\mathrm{QCI}(\mathcal{A},\mathcal{B}) \geqslant 0$; (3) it is a a metric on von Neumann measurements; (4) it is maximal for maximally complementary measurement, such as mutually unbiased bases.

However, in an experimental setting, directly obtaining $\mathrm{Prob}(\hat{A},\mathcal{B})$ is challenging, as the eigenspaces $\{A_i\}$ and $\{B_j\}$ may be unknown. Similarly, measuring $\mathrm{QCI}(\mathcal{A},\mathcal{B})$ directly is infeasible due to the non-symmetric ordering in $\mathrm{Tr}[A_iB_jA_iB_j]$.

Nevertheless, if these two processes occur within a quantum switch, the two possible orderings, $\mathcal{B}(\mathcal{A}(\rho))$ and $\mathcal{A}(\mathcal{B}(\rho))$, take place simultaneously on the input state ρ. According to (3), the probability of obtaining an outcome projecting the control qubit onto $|-\rangle$ is given by the $Z\omega Z$ term, i.e.,

$$p_- = \frac{1}{4}\sum_{ij}\mathrm{Tr}\left(\rho\big|[A_i,B_j]\big|^2\right), \tag{9}$$

where $\big|[A_i,B_j]\big|^2 = [A_i,B_j]^\dagger[A_i,B_j]$. When the two processes are nearly identical, the '$-$' state also corresponds to the dark port, where destructive interference occurs.

A key observation is that, for an input state $\rho = \frac{1}{d}I$, the QCI can be directly inferred from the measurement of the control qubit as

$$\mathrm{QCI}(\mathcal{A},\mathcal{B}) = \sqrt{2p_-}. \tag{10}$$

This result highlights an important application of the quantum switch: beyond demonstrating computational advantages for unitary quantum channels, control qubit measurements also provide a practical method for characterizing the QCI.

From a statistical perspective, using indefinite causal order to estimate QCI offers significant advantages in scalability. This is because QCI can be directly extracted from the measurement statistics of the control qubit. Specifically, if let $\hat{p}_-$ denote the empirical estimate of the control qubit probability, it follows a binomial distribution. By applying Hoeffding's inequality, we find that to ensure the estimated probability deviates from the true value by no more than ϵ with confidence at least $1-\delta$, the required number of experimental shots satisfies

$$n \geqslant -\frac{1}{2\epsilon}\log\frac{\delta}{2}. \tag{11}$$

Notably, Eq. (11) reveals that the required sample size is independent of the system's Hilbert space dimension d, making this approach especially advantageous for high-dimensional systems. Furthermore, we show that even in the simplest case with $d=2$, the ICO-based method outperforms indirect approaches such as full process tomography in terms of efficiency and accuracy for estimating QCI.

4 Experimental setup

The experimental setup used for measuring the QCI is illustrated in Figure 1. Single photons are generated via spontaneous parametric down-conversion (SPDC) in a periodically poled KTP (ppKTP) crystal. The SPDC process produces a pair of entangled photons, one signal photon, and one idler photon. The signal photon is sent directly to a single-photon detector (SPD) for detection, while the idler photon travels through the experimental setup via fiber optics. Initially, the idler photon passes through a fiber circulator and is then injected into a 2×2 fiber beam splitter (FBS). This FBS applies a Hadamard operation on the path degree of freedom (DOF), which is essential for preparing the state of the system. Specifically, the Hadamard operation on the path DOF of the idler photon creates an equal superposition of the control qubit (C) states, $|0\rangle_C$ and $|1\rangle_C$. The state is then described as

$$|\phi\rangle_T \otimes \frac{1}{\sqrt{2}}(|0\rangle_C + |1\rangle_C), \tag{12}$$

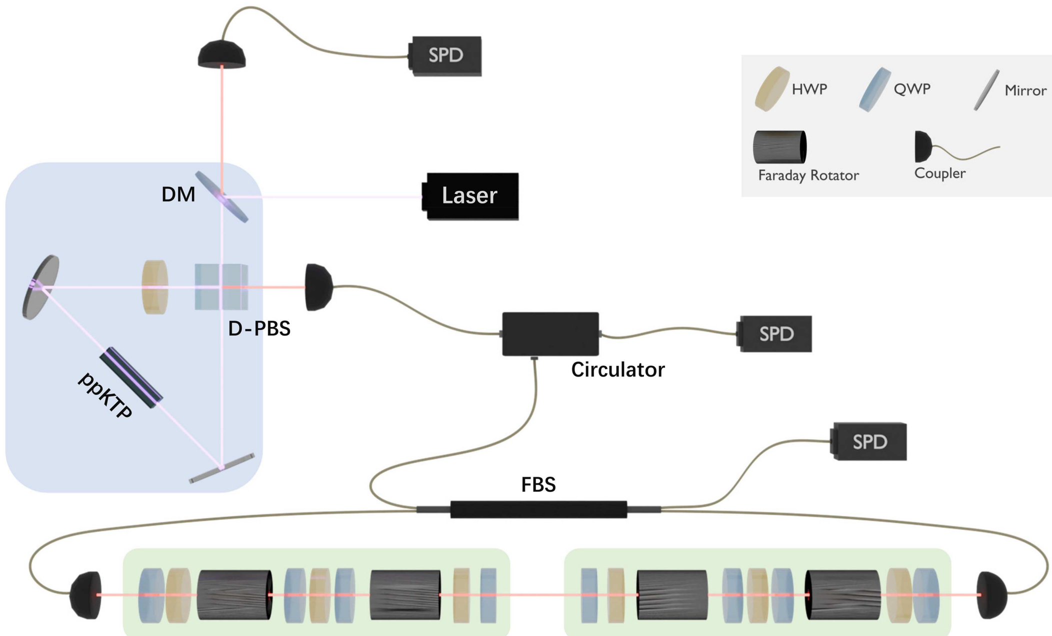

Figure 1 (Color online) Experimental setup. Single photons are generated via type-II spontaneous parametric down-conversion (SPDC) using a periodically poled KTP (ppKTP) crystal, as highlighted by the blue region. This crystal, pumped by a laser at a wavelength of $\lambda_p = 404$ nm, produced photon pairs with a wavelength of $\lambda_s = \lambda_i = 808$ nm. The pump beam and the down-converted photons are separated by using a dual-wavelength polarizing beam splitter (DPBS) and a dichroic mirror (DM). The signal photon heralds the idler photon, which propagates through the quantum switch. Photon detection is performed by using single-photon detectors (SPDs). The idler photon successively passes through a circulator, a fiber beam splitter (FBS), and two reciprocal unitaries (highlighted by the green region). The output ports of FBS in the backward direction are connected to two SPDs, while the photons exiting through the outputs overlapping with the input port are separated by the fiber circulator.

where the target qubit (T) corresponds to the polarization DOF of the photon, and $|\phi\rangle_T$ denotes the polarization state. After the initial superposition state is prepared, the photon enters a free-space optical loop containing polarization devices that implement two reciprocal unitary operations (which will be detailed in the Supplementary File), labeled A and B. The polarization devices were placed between two couplers. As the photon traverses the loop, it undergoes both sequences AB and BA in a coherent superposition, effectively correlating the operation order with the control qubit state. After passing through the polarization devices, the photon returns to the FBS, where resulting states at two outputs are given by

$$\begin{aligned} |\Phi_+\rangle &= \frac{1}{2}(AB + BA)\,|\phi_T\rangle\,, \\ |\Phi_-\rangle &= \frac{1}{2}(AB - BA)\,|\phi_T\rangle\,. \end{aligned} \tag{13}$$

These two output states correspond to the constructive and destructive interference patterns arising from the commutation or anti-commutation of the operations A and B. Their respective probabilities are measured by SPDs connected to the output ports of the FBS, allowing for the evaluation of the QCI.

5 Experimental results

In this section, we analyze the behavior of QCI under various quantum channels, specifically focusing on depolarizing, bit-flip, and phase-flip channels, as well as unitary operations such as the Pauli operators X, Y, Z, and the identity I. The QCI for two unknown observables can be directly estimated from experimental data, in particular from the probability distribution of the '$-$' outcome. Prior to performing the QCI measurement tasks, our experimental setup achieved high interferometric visibility, exceeding 0.9972. At the end of this section, we present a comparative analysis between our proposed scheme and the conventional process tomography approach. The results clearly demonstrate that our method offers substantial advantages in resource efficiency, achieving comparable accuracy in QCI estimation while requiring significantly fewer photons.

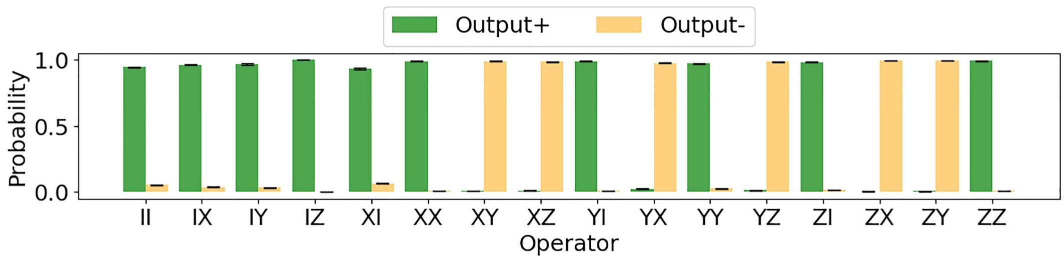

Figure 2 (Color online) Probabilities of photon detection at the commutator and anti-commutator ports of the quantum switch for each pair of unitary operators (A, B) from the set $\{X, Y, Z, I\}$. Theoretical probabilities take values $p \in \{0, 1\}$, while the experimentally observed probabilities are shown as bars in the figure. The x-axis labels indicate the specific pair of unitary operators (A, B). Green bars represent the probability of detecting output '+' from the FBS, and yellow bars represent the probability of detecting output '−'.

5.1 Both channels are unitary channels

To certify that our experimental platform is capable of realizing indefinite causal order in the Sagnac configuration, we first analyze the behavior of QCI when both channels are unitary operations. We select A and B such that each represents one of the Pauli operators, i.e., $\{A, B\} \in \{X, Y, Z, I\}$. According to (1), we can determine whether the gates (A, B) commute or anti-commute for several different input states by measuring the photon's exit port. We then analyze the probability distribution of photon counts at the two output ports of the FBS. The corresponding results are shown in Figure 2. If the gates commute, the photon is ideally expected to exit port '−' of the FBS, while if they anti-commute, it should exit port '+'. The average success rate (i.e., the probability of the photon exiting the theoretically correct port) across all tested operator pairs is 0.981 ± 0.016.

5.2 Both channels are noise channels

We now analyze the behavior of QCI when both channels are noisy. We consider three types of noise channels: depolarizing, bit-flip, and phase-flip. Each channel is characterized by a noise probability p, with corresponding Kraus representations. The Kraus representation for the depolarizing channel is provided in the following form:

$$K_0 = \sqrt{1-p}I, K_1 = \sqrt{\frac{p}{3}}X, K_2 = \sqrt{\frac{p}{3}}Y, K_3 = \sqrt{\frac{p}{3}}Z. \tag{14}$$

The Kraus representation for the bit-flip channel is provided in the following form:

$$K_0 = \sqrt{1-p}I, K_1 = \sqrt{p}X. \tag{15}$$

The Kraus representation for the phase-flip channel is provided in the following form:

$$K_0 = \sqrt{1-p}I, K_1 = \sqrt{p}Z. \tag{16}$$

Here, X, Y, and Z denote the standard Pauli matrices, respectively, and I denotes the identity operator. Specifically, the Pauli operators are given by $X = |0\rangle\langle 1| + |1\rangle\langle 0|$, $Y = i(|1\rangle\langle 0| - |0\rangle\langle 1|)$, and $Z = |0\rangle\langle 0| - |1\rangle\langle 1|$.

Consider the case where both channel $\mathcal{A}$ and channel $\mathcal{B}$ are depolarizing channels. Let the parameters p_a and p_b denote the depolarizing probabilities for channel $\mathcal{A}$ and channel $\mathcal{B}$, respectively. At this stage, the value of $\mathrm{QCI}(\mathcal{A}, \mathcal{B})$ assumes the following form (more details are shown in the Supplementary File):

$$\mathrm{QCI}(\mathcal{A}, \mathcal{B}) = \sqrt{2p_-} = \sqrt{\frac{4}{3}p_a p_b}, \tag{17}$$

where p_- represents the probability of the outcome '−'. When p_a and p_b are different values, the theoretical and experimental values of QCI are shown in Figure 3(a). Theoretical predictions are depicted as solid lines, while experimental data are represented by discrete dots. Each colored line indicates the variation of QCI as a function of p_a (x-axis) for a fixed value of p_b. Notably, when $p_b = 0$ (or $p_a = 0$), the corresponding channel $\mathcal{B}$ (or $\mathcal{A}$) effectively becomes an identity channel. An identity channel preserves

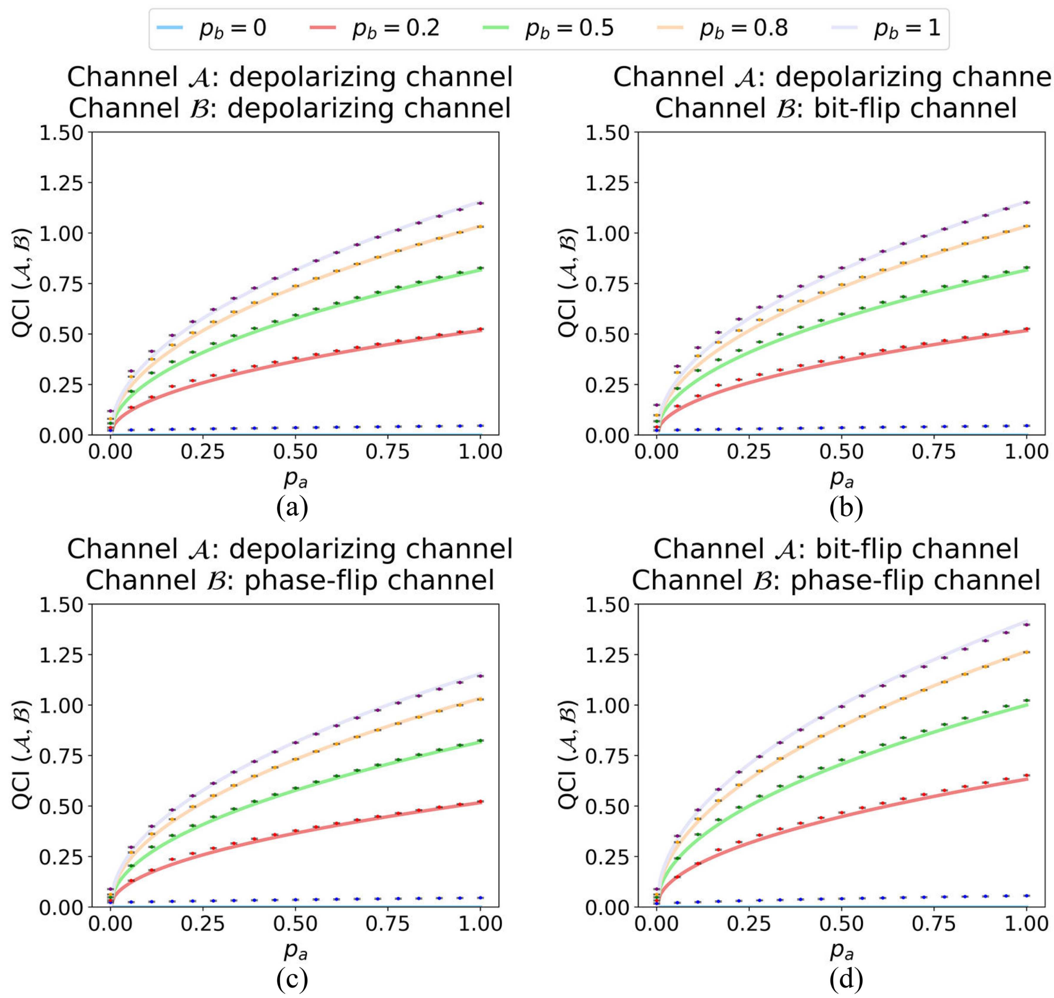

Figure 3 (Color online) Theoretical and experimental results of the QCI under combinations when both $\mathcal{A}$ and $\mathcal{B}$ channels are both noisy quantum channels. Parameters p_a and p_b denote the noise probabilities of channels $\mathcal{A}$ and $\mathcal{B}$, respectively. The x-axis represents p_a, and each curve corresponds to a different fixed value of p_b as indicated by the different colors. Solid lines represent theoretical predictions; experimental data points are shown as dots with error bars representing standard uncertainties. (a) The variation of QCI when channel $\mathcal{A}$ and channel $\mathcal{B}$ are both depolarizing channels; (b) the variation of QCI when channel $\mathcal{A}$ is the depolarizing channel and channel $\mathcal{B}$ is the bit-flip channel; (c) the variation of QCI when channel $\mathcal{A}$ is the depolarizing channel and channel $\mathcal{B}$ is the phase-flip channel; (d) the variation of QCI when channel $\mathcal{A}$ is the bit-flip channel and channel $\mathcal{B}$ is the phase-flip channel.

the eigenstates associated with the observable of the other channel, thereby avoiding any disturbance or collapse of the quantum state. In such cases, the observables of channels $\mathcal{A}$ and $\mathcal{B}$ are compatible, and thus, the theoretical value of QCI remains zero. Experimentally, when $p_a = p_b = 0$, the measured value of QCI is 0.031, which is close to the expected theoretical value of zero. Conversely, when both p_a and p_b equal 1, the channels $\mathcal{A}$ and $\mathcal{B}$ function as fully depolarizing channels, and the QCI reaches its theoretical maximum value of $\sqrt{\frac{4}{3}} \approx 1.1547$. The corresponding experimental value is 1.149, demonstrating strong agreement with theoretical predictions.

Consider the scenario where both channel $\mathcal{A}$ and channel $\mathcal{B}$ are either bit-flip channels or phase-flip channels. The detailed procedure for calculating QCI is provided in the Supplementary File. In this case, the value of $\mathrm{QCI}(\mathcal{A}, \mathcal{B})$ satisfies the following equation:

$$\mathrm{QCI}(\mathcal{A}, \mathcal{B}) = \sqrt{2p_-} = 0. \tag{18}$$

The vanishing value of p_- arises from the fact that the commutation relation $[A_i, B_j] = 0$ holds for all i, j. This indicates that the observables associated with channels $\mathcal{A}$ and $\mathcal{B}$ commute, and hence, no measurement-induced disturbance is introduced by either channel. Consequently, the value of QCI remains identically zero for all combinations of bit-flip (or phase-flip) probabilities in channels $\mathcal{A}$ and $\mathcal{B}$.

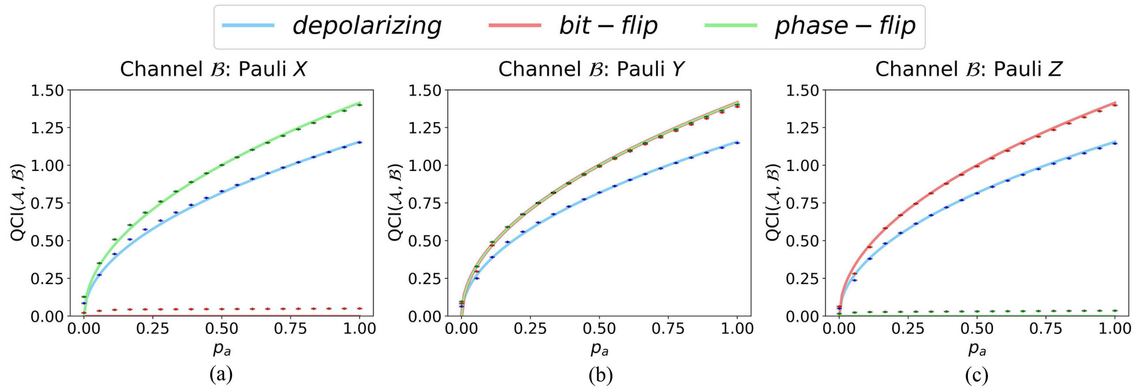

Figure 4 (Color online) Theoretical and experimental results of the QCI under combinations of quantum channels, with one channel being a Pauli operation. In each subfigure, the horizontal axis indicates the noise strength p_a of channel $\mathcal{A}$, while channel $\mathcal{B}$ is fixed as a unitary channel corresponding to a Pauli operator: (a) X, (b) Y, and (c) Z. For each plot, channel $\mathcal{A}$ is implemented as a depolarizing channel (blue), a bit-flip channel (red), or a phase-flip channel (green). Solid lines represent theoretical predictions; dots correspond to experimental data. Error bars indicate the standard deviation of the measured QCI values. The results illustrate how QCI varies with p_a under different noise models for channel $\mathcal{A}$ and fixed unitary operations in channel $\mathcal{B}$.

In the scenario where one channel is a depolarizing channel and the other is either a bit-flip or phase-flip channel, the QCI values for these configurations are given by

$$\mathrm{QCI}(\mathcal{A},\mathcal{B}) = \sqrt{2p_-} = \sqrt{\frac{4}{3}p_a p_b}. \tag{19}$$

As seen in Figures 3(b) and (c), the QCI values increase with both p_a and p_b, reaching a maximum value when both channels are fully depolarizing and flipping. The experimental data aligns well with the theoretical predictions, further validating the model.

In the scenario where one of the channels is a bit-flip channel and the other is a phase-flip channel, the QCI expression is

$$\mathrm{QCI}(\mathcal{A},\mathcal{B}) = \sqrt{2p_-} = \sqrt{2p_a p_b}. \tag{20}$$

This configuration is illustrated in Figure 3(d). Without loss of generality, let channel $\mathcal{A}$ be the bit-flip channel and channel $\mathcal{B}$ be the phase-flip channel. In this setting, p_a and p_b denote the bit-flip probability of channel $\mathcal{A}$ and the phase-flip probability of channel $\mathcal{B}$, respectively. A similar trend is demonstrated in that QCI reaches its theoretical maximum when both probabilities are set to 1, with experimental results matching theoretical expectations.

Overall, the experimental results exhibit strong consistency with the theoretical predictions across the entire range of tested parameters.

5.3 Unitary channel and noise channels

In this section, we investigate the theoretical and experimental behavior of the QCI when one of the channels is a noisy quantum channel, such as a depolarizing, bit-flip, or phase-flip channel, and the other is a unitary channel corresponding to one of the Pauli operators X, Y, Z. These Pauli operations represent fundamental types of unitary transformations and play a central role in quantum information theory. Specifically, we analyze the variation of the QCI as a function of the noise strength of channel $\mathcal{A}$, denoted by the parameter p_a, while fixing channel $\mathcal{B}$ as a unitary channel that applies one of the Pauli operators X, Y, Z. As shown in Figure 4, we examine the following cases. In Figure 4(a), Channel $\mathcal{B}$ is fixed as the X operator, while channel $\mathcal{A}$ takes on different forms: depolarizing (blue), bit-flip (red), and phase-flip (green) channels. The horizontal axis represents the noise parameter p_a of channel $\mathcal{A}$, and the vertical axis indicates the corresponding QCI value. Theoretical predictions are shown as solid lines, and experimental results are plotted as discrete points with error bars representing standard deviations. In Figures 4(b) and (c), these subfigures present analogous results for channel $\mathcal{B}$ fixed as the Y and Z operators, respectively. Again, channel $\mathcal{A}$ is varied among depolarizing, bit-flip, and phase-flip channels, and the QCI is presented using the same color scheme. The results reveal that the QCI increases with the noise strength p_a, and the nature of this increase depends on both the type of noise introduced by channel

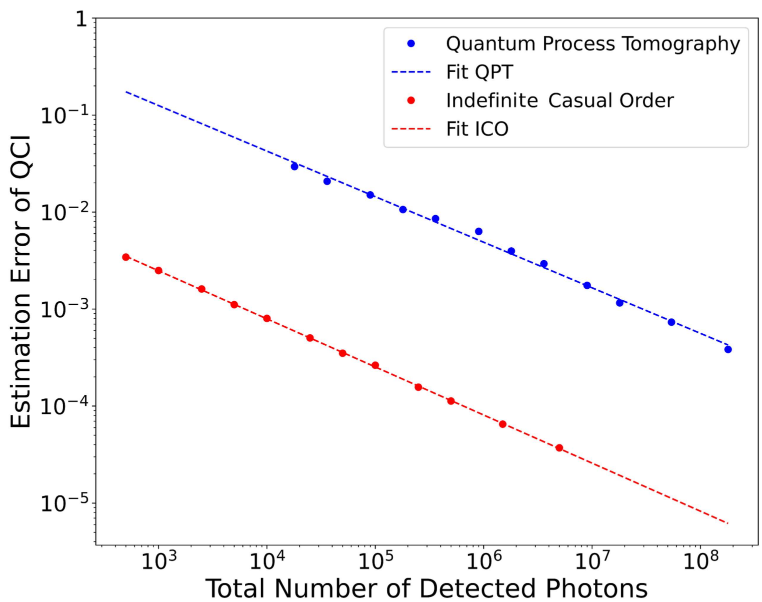

Figure 5 (Color online) Comparison of the estimation error between ICO-based method vs. QPT-based method. Comparison of the estimation error of QCI between identity channel and Pauli-X channel, as a function of photon consumption. The horizontal axis shows the number of photons used, while the vertical axis indicates the absolute estimation error. Red points represent our ICO-based method, while blue points represent the conventional QPT-based approach. The ICO-based method achieves approximately 18 dB lower estimation error for the same number of photons, corresponding to a nearly 50-fold improvement in accuracy. This demonstrates the significant resource efficiency of our approach, especially in the low-photon regime.

$\mathcal{A}$ and the specific unitary transformation applied by channel $\mathcal{B}$. Since depolarizing noise affects any state on the Bloch sphere isotropically, the resulting QCI exhibits similar trends for all three Pauli operators. In contrast, the bit-flip (red) and phase-flip (green) channels introduce direction-dependent decoherence. As a result, the QCI is more sensitive to the commutation relations between the Pauli operator of channel $\mathcal{B}$ and the Kraus operators of channel $\mathcal{A}$. As expected, when the observables associated with the two channels commute, for example, the Z operator and the phase-flip channel, the QCI remains close to zero due to the absence of measurement-induced disturbance. Conversely, when the observables do not commute, the QCI assumes larger values, reflecting the incompatibility between measurements associated with the two channels. Across all configurations, the experimental results are in strong agreement with theoretical predictions, thereby validating the theoretical framework and confirming the accuracy of our experimental implementation.

5.4 Convergence advantage over conventional methods

In this section, we compare the convergence behavior of our ICO-based approach with that of the conventional estimation method based on quantum process tomography (QPT). Specifically, we demonstrate that our scheme achieves significantly lower estimation error with substantially fewer resources.

The conventional QPT-based method refers to the standard two-step procedure: first reconstructing the process matrices of the quantum channels via tomography, and then computing the degree of non-commutativity between the reconstructed channels to estimate the QCI. In contrast, our method extracts the QCI directly from control qubit measurements in an indefinite causal order setup, bypassing full process reconstruction.

To quantitatively illustrate the advantage, we consider a representative scenario involving two qubit channels: the identity channel $\mathcal{I}$ and the Pauli-X channel, acting on a two-dimensional Hilbert space ($d = 2$). The estimation performance is compared in Figure 5, where the horizontal axis denotes the number of photons used (i.e., the number of experimental shots), and the vertical axis indicates the absolute estimation error of the QCI.

Our results reveal a clear advantage for the ICO-based scheme. While both methods follow a power-law scaling with respect to the number of photons, fitting the error data in a log-log plot yields the following relations:

$$\begin{cases} \log_{10}(Err.) = -0.5\log_{10}(N) + 0.708, & \text{(QPT)}, \\ \log_{10}(Err.) = -0.5\log_{10}(N) - 1.093, & \text{(ICO)}. \end{cases} \tag{21}$$

This corresponds to an error reduction of approximately 18 dB in favor of our ICO-based method, meaning that for the same photon count, our scheme achieves nearly 50 times lower estimation error.

This substantial improvement highlights the efficiency and scalability of our protocol, particularly in resource-constrained scenarios. The ability to directly access QCI from control qubit statistics, without the need for full process tomography, demonstrates the practical benefits of indefinite causal order for quantum channel characterization.

6 Discussion

Our work presents an experimental realization of measuring QCI within a Sagnac-interferometer-based quantum switch. By leveraging indefinite causal order, we demonstrate an approach that surpasses conventional methods relying solely on sequential applications of channels. The results confirm the ability of the quantum switch to distinguish incompatible channels effectively, offering a practical tool for investigating quantum channel properties.

This experiment not only introduces a new technique for quantifying QCI but also showcases how the quantum switch can serve as a powerful tool for probing fundamental quantum properties. The ability to exploit indefinite causal order for measuring incompatibility may have profound implications for quantum information science, particularly in areas such as quantum communication and resource characterization.

Future work may extend this protocol to higher-dimensional systems and other physical platforms, broadening the scope of quantum technologies that can benefit from this approach. Our findings reinforce the significance of the quantum switch in unlocking novel functionalities that may be instrumental in next-generation quantum applications.

Acknowledgements This work was supported by Innovation Program for Quantum Science and Technology (Grant Nos. 2021ZD0301200, 2021ZD0301400, 2021ZD0300702, 2021ZD0301201), National Natural Science Foundation of China (Grant Nos. 12350006, 12075323), and USTC Research Funds of the Double First-Class Initiative (Grant No. YD2030002026).

Supporting information The supporting information is available online at info.scichina.com and link.springer.com. The supporting materials are published as submitted, without typesetting or editing. The responsibility for scientific accuracy and content remains entirely with the authors.

References

1 Bohr N. The quantum postulate and the recent development of atomic theory. Nature, 1928, 121: 580–590
2 Bell J S. On the Einstein Podolsky Rosen paradox. Phys Physique Fizika, 1964, 1: 195–200
3 Brunner N, Cavalcanti D, Pironio S, et al. Bell nonlocality. Rev Mod Phys, 2014, 86: 419–478
4 Quintino M T, Vértesi T, Brunner N. Joint measurability, Einstein-Podolsky-Rosen steering, and bell nonlocality. Phys Rev Lett, 2014, 113: 160402
5 Kochen S, Specker E. The problem of hidden variables in quantum mechanics. Inda Univ Math J, 1967, 17: 59–87
6 Budroni C, Cabello A, Gühne O, et al. Kochen-Specker contextuality. Rev Mod Phys, 2022, 94: 045007
7 Spekkens R W. Contextuality for preparations, transformations, and unsharp measurements. Phys Rev A, 2005, 71: 052108
8 Heisenberg W. Über den anschaulichen Inhalt der quantentheoretischen kinematik und mechanik. Z Physik, 1927, 43: 172–198
9 Ozawa M. Universally valid reformulation of the Heisenberg uncertainty principle on noise and disturbance in measurement. Phys Rev A, 2003, 67: 042105
10 Ozawa M. Physical content of Heisenberg's uncertainty relation: limitation and reformulation. Phys Lett A, 2003, 318: 21–29
11 Ozawa M. Uncertainty relations for noise and disturbance in generalized quantum measurements. Ann Phys, 2004, 311: 350–416
12 Ozawa M. Universal uncertainty principle in the measurement operator formalism. J Opt B-Quantum Semiclass Opt, 2005, 7: S672–S681
13 Busch P, Heinosaari T, Schultz J, et al. Comparing the degrees of incompatibility inherent in probabilistic physical theories. Europhys Lett, 2013, 103: 10002
14 Haapasalo E. Robustness of incompatibility for quantum devices. J Phys A-Math Theor, 2015, 48: 255303
15 Uola R, Budroni C, Gühne O, et al. One-to-one mapping between steering and joint measurability problems. Phys Rev Lett, 2015, 115: 230402
16 Pusey M F. Verifying the quantumness of a channel with an untrusted device. J Opt Soc Am B, 2015, 32: 56–63
17 Wang X, Wilde M M. Resource theory of asymmetric distinguishability for quantum channels. Phys Rev Res, 2019, 1: 033169
18 Carmeli C, Heinosaari T, Toigo A. Quantum Incompatibility Witnesses. Phys Rev Lett, 2019, 122: 130402
19 Leppäjärvi L, Sedlák M. Incompatibility of quantum instruments. Quantum, 2024, 8: 1246
20 Girard M, Plávala M, Sikora J. Jordan products of quantum channels and their compatibility. Nat Commun, 2021, 12: 2129
21 Guo Y, Luo S, Zhang L. Quantifying channel incompatibility via Jordan negativity. Phys Lett A, 2025, 543: 130444
22 Rozema L A, Darabi A, Mahler D H, et al. Violation of Heisenberg's measurement-disturbance relationship by weak measurements. Phys Rev Lett, 2012, 109: 100404
23 Baek S Y, Kaneda F, Ozawa M, et al. Experimental violation and reformulation of the Heisenberg's error-disturbance uncertainty relation. Sci Rep, 2013, 3: 2221

24 Erhart J, Sponar S, Sulyok G, et al. Experimental demonstration of a universally valid error-disturbance uncertainty relation in spin measurements. Nat Phys, 2012, 8: 185–189
25 Kaneda F, Baek S Y, Ozawa M, et al. Experimental test of error-disturbance uncertainty relations by weak measurement. Phys Rev Lett, 2014, 112: 020402
26 Weston M M, Hall M J W, Palsson M S, et al. Experimental test of universal complementarity relations. Phys Rev Lett, 2013, 110: 220402
27 Ringbauer M, Biggerstaff D N, Broome M A, et al. Experimental joint quantum measurements with minimum uncertainty. Phys Rev Lett, 2014, 112: 020401
28 Procopio L M, Moqanaki A, Araújo M, et al. Experimental superposition of orders of quantum gates. Nat Commun, 2015, 6: 7913
29 Rubino G, Rozema L A, Feix A, et al. Experimental verification of an indefinite causal order. Sci Adv, 2017, 3: e1602589
30 Goswami K, Giarmatzi C, Kewming M, et al. Indefinite causal order in a quantum switch. Phys Rev Lett, 2018, 121: 090503
31 Guo Y, Hu X M, Hou Z B, et al. Experimental transmission of quantum information using a superposition of causal orders. Phys Rev Lett, 2020, 124: 030502
32 Rubino G, Rozema L A, Ebler D, et al. Experimental quantum communication enhancement by superposing trajectories. Phys Rev Res, 2021, 3: 013093
33 Cao H, Bavaresco J, Wang N N, et al. Semi-device-independent certification of indefinite causal order in a photonic quantum switch. Optica, 2023, 10: 561–568
34 Gao N, Li D, Mishra A, et al. Measuring incompatibility and clustering quantum observables with a quantum switch. Phys Rev Lett, 2023, 130: 170201
35 Wei K, Tischler N, Zhao S R, et al. Experimental quantum switching for exponentially superior quantum communication complexity. Phys Rev Lett, 2019, 122: 120504
36 Yin P, Zhao X, Yang Y, et al. Experimental super-Heisenberg quantum metrology with indefinite gate order. Nat Phys, 2023, 19: 1122–1127
37 Cao H, Wang N N, Jia Z, et al. Quantum simulation of indefinite causal order induced quantum refrigeration. Phys Rev Res, 2022, 4: L032029
38 Chiribella G, D'Ariano G M, Perinotti P, et al. Quantum computations without definite causal structure. Phys Rev A, 2013, 88: 022318